International Journal of Heat and Mass Transfer 53 (2010) 2218–2228

Contents lists available at ScienceDirect

International Journal of Heat and Mass Transfer

journal homepage: www.elsevier.com/locate/ijhmt

Experimental study of R-134a evaporation heat transfer in a narrow annular duct

C.A. Chen, C.Y. Lee, T.F. Lin *

Department of Mechanical Engineering, National Chiao Tung University, Hsinchu, 1001 Ta Hsueh Road, Hsinchu 30010, Taiwan

ARTICLE INFO

Article history:
Received 8 October 2009
Received in revised form 18 November 2009
Accepted 18 November 2009
Available online 22 January 2010

Keywords:
R-134a
Evaporation heat transfer
Mini-channel
Evaporating flow pattern

ABSTRACT

An experiment is carried out here to investigate the evaporation heat transfer and associated evaporating flow pattern for refrigerant R-134a flowing in a horizontal narrow annular duct. The gap of the duct is fixed at 1.0 and 2.0 mm. In the experiment, the effects of the duct gap, refrigerant vapor quality, mass flux and saturation temperature and imposed heat flux on the measured evaporation heat transfer coefficient h_r are examined in detail. For the duct gap of 2.0 mm, the refrigerant mass flux G is varied from 300 to 500 kg/m^2 s, imposed heat flux q from 5 to 15 kW/m^2, vapor quality $\boldsymbol{x}_m$ from 0.05 to 0.95, and refrigerant saturation temperature T_{sat} from 5 to 15 °C. While for the gap of 1.0 mm, G is varied from 500 to 700 kg/m^2 s with the other parameters varied in the same ranges as that for $\delta = 2.0$ mm. The experimental data clearly show that the evaporation heat transfer coefficient increases almost linearly with the vapor quality of the refrigerant and the increase is more significant at a higher G. Besides, the evaporation heat transfer coefficient also rises substantially at increasing q. Moreover, a significant increase in the evaporation heat transfer coefficient results for a rise in T_{sat}, but the effects are less pronounced in the narrower duct at a low imposed heat flux and a high refrigerant mass flux. Furthermore, the evaporation heat transfer coefficient increases substantially with the refrigerant mass flux except at low vapor quality. We also note that reducing the duct gap causes a significant increase in h_r. In addition to the heat transfer data, photos of R-134a evaporating flow taken from the duct side show the change of the dominant two-phase flow pattern in the duct with the experimental parameters. Finally, an empirical correlation for the present measured heat transfer coefficient for the R-134a evaporation in the narrow annular ducts is proposed.

1. Introduction

In air-conditioning system design, the refrigerant chosen to be used in the refrigeration loop is known to play an important role. The hydrochlorofluorocarbons refrigerants (HCFCs) such as refrigerant R-22 and the chlorofluorocarbons refrigerants (CFCs) such as refrigerants R-11, R-12, R-113, R-114 and R-115 have been employed for many years. However, the chlorine ions contained in these refrigerants have resulted in the destruction of the ozone layer in the arctic area and the global warming. Thus the Montreal Protocol signed in 1987 only allowed the use of the CFCs up to 1996. Besides, the HCFCs are going to be phased out in 2020. Consequently, the search for the replacement of CFCs and HCFCs becomes very urgent. Various non-chlorine alternative refrigerants such as R-134a, R-290, R-401A, R-407C and R-410A have been considered to be suitable and some are currently in use.

It is well known that R-134a is a single-component HFC refrigerant and has similar thermophysical properties to R-12. Hence refrigerant R-134a has been extensively used currently in many refrigeration and air-conditioning systems to replace R-12 and R-22.

In many air-conditioning systems, using small channels is a good choice because of their low thermal resistance, very high ratio of surface area to volume, low inventory, small volumes and lower total mass of working fluids. Thus the use of compact heat-exchangers consisting of small channels to promote the thermal performance of these systems is beneficial. The understanding of the evaporation heat transfer characteristics of R-134a in small channels is therefore needed.

The size of the channels in a compact heat exchanger can significantly affect the performance of the exchanger, suggesting that the channel confinement effects on the two-phase flow in the exchanger are important. In classifying the channel size Kandlikar et al. [1,2] proposed that Dh > 3 mm for conventional channels, 200 μm < D_h < 3 mm for mini-channels, and 10 μm< D_h < 200 μm for micro-channels. Kew and Cornwell [3] investigated refrigerant R-141b boiling in a horizontal tube with its inner diameter ranging from 1.39 to 3.69 mm and introduced a new dimensionless group named as the Confinement number, $N_{conf} \equiv \frac{[\sigma/(g(\rho_l-\rho_g))]^{1/2}}{D_h}$, which represented the importance of the restriction of the flow by the small size of the channel. They showed that the confined boiling

* Corresponding author. Tel.: +886 35712121; fax: +886 35 726440.
E-mail address: tflin@mail.nctu.edu.tw (T.F. Lin).

0017-9310/$ - see front matter © 2009 Elsevier Ltd. All rights reserved.
doi:10.1016/j.ijheatmasstransfer.2009.12.011

Nomenclature

A_s	outside surface area of the heated inner pipe, m^2
Bo	Boiling number, $Bo = \frac{q}{G \cdot i_{fg}}$, dimensionless
c_p	specific heat, J/kg°C
D_i, D_o	inner and outside diameters of duct, m
D_h	hydraulic diameter, $D_h = (D_o - D_i)$, m
f_f	friction factor
g	acceleration due to gravity, m/s^2
G	mass flux, kg/m^2 s
h_r	evaporation heat transfer coefficient, W/m^2 °C
i_{fg}	enthalpy of vaporization, J/kg
k_l	liquid thermal conductivity, W/m °C
t_{lf}	liquid film thickness, μm
N_{conf}	Confinement number, $N_{conf} = \frac{(\sigma/(g\Delta\rho))^{0.5}}{D_h}$, dimensionless
Nu	Nusselt number, $Nu = \frac{hD_h}{k}$, dimensionless
P	system pressure, kPa
Pr	Prandtl number, $Pr = \frac{\mu \cdot c_p}{k}$, dimensionless
q	average imposed heat flux, W/m^2
Q_n	net power input, W
Re	Reynolds number, $Re = \frac{G \cdot D_h}{\mu_l}$, dimensionless
T_w	wall temperature of heated inner pipe, °C
T_{sat}	saturated temperature of the refrigerant, °C
$\boldsymbol{x}_m$	mean vapor quality
X_{tt}	Martnelli parameter
z	coordinate (downstream coordinate for annular duct flow), mm

Greek symbols

δ	gap size, mm
μ_l	viscosity of liquid R-134a, $N \cdot s/m^2$
ρ_g, ρ_l	vapor and liquid densities, kg/m^3
$\Delta\rho$	density difference, $\Delta\rho = \rho_l - \rho_g$, kg/m^3
σ	surface tension, N/m

occurred when $N_{conf} > 0.5$. Accordingly, the effects of the tube confinement can be significant for two-phase flow in micro- and mini-channels.

In the following the relevant literature on the evaporation heat transfer of refrigerants in conventional and some enhanced tubes is reviewed. Experimental data taken for the evaporation heat transfer characteristics of R-22/R-407C in a smooth tube (D_h = 6.5 mm) by Wang and Chiang [4] for the vapor quality varied from 0.1 to 0.9 showed that the R-22 evaporation heat transfer coefficient increased at increasing mass flux and vapor quality. However, the R-407C evaporation heat transfer coefficient increased at increasing mass flux but decreased at increasing vapor quality. Park and Hrnjak [5] studied CO_2 and R-410A flow boiling heat transfer, pressure drop and flow pattern at low temperatures in a horizontal smooth tube (D_h=6.1 mm). They found that the evaporation heat transfer coefficient of R-410A increased with the mass flux and vapor quality. Besides, the evaporation heat transfer coefficient of CO_2 is higher than R-410A.

A comprehensive review of saturated flow boiling in small passages of compact heat-exchangers conducted by Watel [6] suggests that heat transfer in the evaporation of refrigerants in small channels is dominated by conduction and convection through the liquid film and the interfacial vaporization. The evaporation heat transfer coefficient depends mainly on the refrigerant mass flux and vapor quality. Evaporation heat transfer and pressure drop of refrigerant R-134a in a bank of 28 small pipes (D_h=2.0 mm) were experimentally investigated by Yan and Lin [7,8]. They reported that the evaporation heat transfer coefficient increased with increasing heat flux at low vapor quality and with T_{sat}. But an opposite trend prevails at high quality. Yun et al. [9] studied evaporation heat transfer characteristics of CO_2 in small channels (D_h = 1.08 and 1.54 mm). Their results indicate that before the liquid film dryout the evaporation heat transfer coefficient increased with heat flux. Besides, the evaporation heat transfer coefficient increases with increasing refrigerant saturated temperature and decreasing channel hydraulic diameter. Moreover, the CO_2 evaporation heat transfer coefficient is higher than R-134a by 53%. An experimental study carried out by Lie et al. [10] to examine the evaporation heat transfer of refrigerants R-134a and R-407C in horizontal banks of small tubes (D_h = 0.83 and 2.0 mm) for $\boldsymbol{x}_m$ ranging from 0.2 to 0.8 showed that the evaporation heat transfer coefficient increased at increasing heat flux, saturated temperature and mass flux. Besides, h_r increases almost linearly with the vapor quality. Evaporative heat transfer and pressure drop of R-410A in small channels (D_h = 1.33 and 1.44 mm) investigated by Yun et al. [11] showed that before the dryout, the evaporation heat transfer coefficient was independent of the refrigerant saturated temperature and mass flux. But after the dryout the evaporation heat transfer coefficient increased at increasing refrigerant saturated temperature, heat flux and mass flux. Choi et al. [12] studied the flow boiling heat transfer of R-22, R-134a and CO_2 in horizontal mini-channels (D_h = 1.5 and 3.0 mm) and reported that the heat transfer coefficient increased with the heat flux. Besides, the dryout quality becomes lower for a higher heat flux.

The above literature review clearly indicates that the experimental data for the evaporation heat transfer of HFC refrigerants in small tubes are still rare. In this investigation we conduct an experiment to measure the evaporation heat transfer coefficient and visualize the associated evaporating flow of refrigerant R-134a in a horizontal narrow annular duct. The effects of the refrigerant vapor quality, saturated temperature, mass flux and imposed heat flux on the evaporation heat transfer and evaporating flow in the duct will be examined in detail.

2. Experimental apparatus and procedures

The experimental system modified slightly from that used in the previous study [13] is employed here to investigate the evaporation heat transfer of R-134a in a narrow annular duct. It is schematically depicted in Fig. 1. The experimental apparatus consists of three main loops, namely, a refrigerant loop, a water–glycol loop and a hot-water loop. Refrigerant R-134a is circulated in the refrigerant loop. In order to control various test conditions of the refrigerant in the test section, we need to control the temperature and flow rate in the other two loops. Here the system is only briefly described. The detailed description is available in the previous study [13].

The test section of the experimental apparatus is a horizontal annular duct with the outer pipe made of Pyrex glass to permit the visualization of two-phase pattern in the evaporating refrigerant flow. The outer Pyrex glass pipe is 160-mm long and 4-mm thick with the inside diameter of 20 mm. Both ends of the pipe are connected with copper tubes of the same size by means of flanges and are sealed by O-rings. The inner smooth pipe has 16.0 or 18.0 mm nominal outside diameter (the pipe wall thickness is 1.75 or 2.75 mm) and is 0.41 m long, so that the hydraulic diameter of the annular duct D_h is 4.0 or 2.0 mm (corresponding to the gap size of 2.0 or 1.0 mm for the duct). In order to insure the gap between the inner and outer pipes being uniform, we first measure

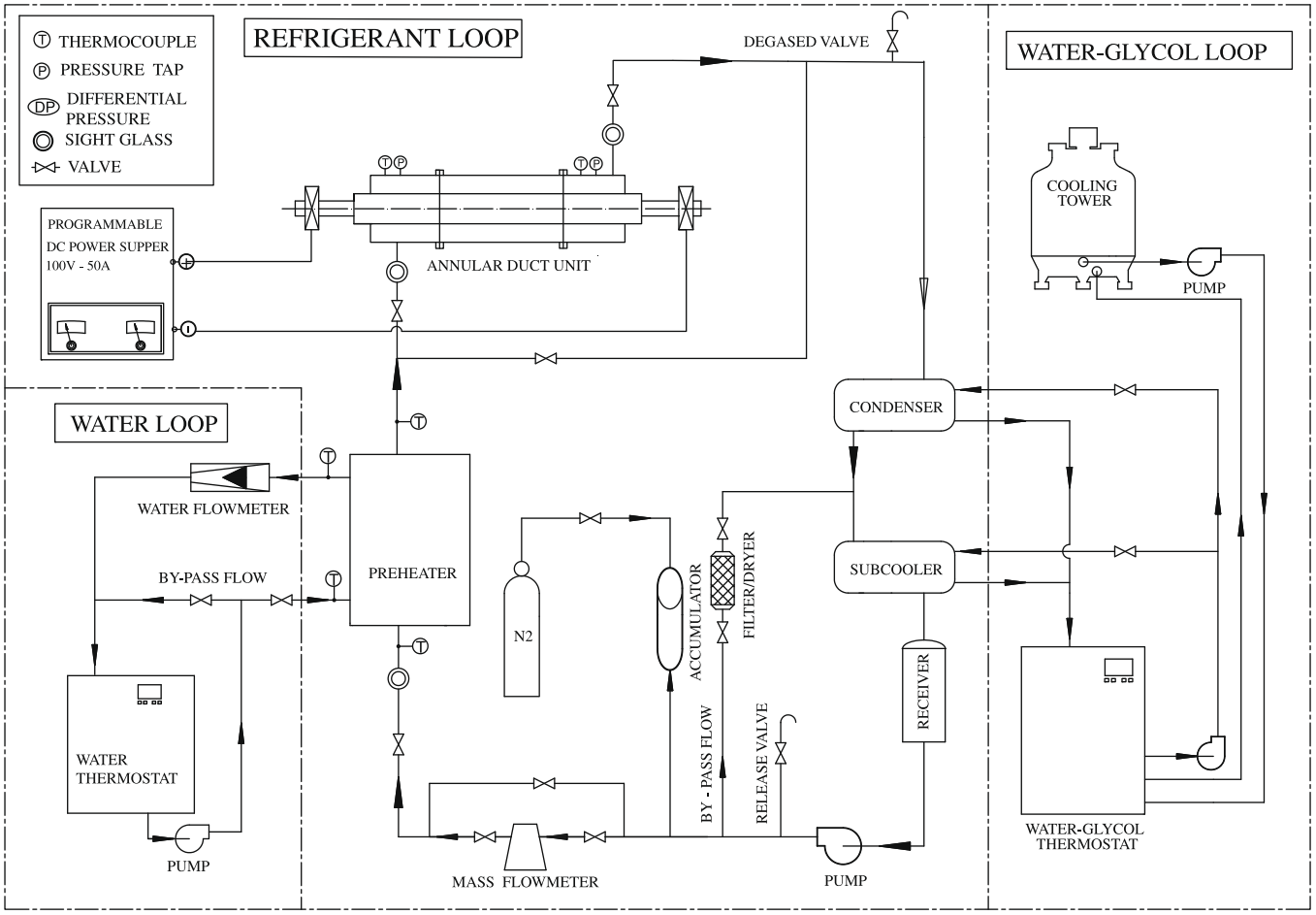

Fig. 1. Schematic of experimental system for the annular duct.

the outside diameter of the inner pipe and the inside diameter of the glass pipe by digital calipers whose resolutions are 0.001 mm with the accuracy of ±0.01 mm. Then we photo the top and side view pictures of the annular duct and measure the average radial distance from the inside surface of the glass pipe to the outside surface of the inner tube. From the above procedures the duct gap is ascertained and its uncertainty is estimated to be 0.019 mm. An electric cartridge heater of 160 mm in length and 12.5 mm in diameter with a maximum power output of 800 W is inserted into the inner pipe. Furthermore, the pipe has an inactive heating zone of 10-mm long at each end and is insulated with Teflon blocks and thermally nonconducting epoxy to minimize heat loss from it. Thermal contact between the heater and the inner pipe is improved by coating a thin layer of heat-sink compound on the heater surface before the installation of the heater. Then, 8 T-type calibrated thermocouples are electrically insulated by electrically nonconducting thermal bond before they are fixed on the inside surface of the inner pipe so that the voltage signals from the thermocouples are not interfered with the DC current passing through the cartridge heater. The thermocouples are positioned at three axial stations along the inner pipe. At each axial station, two to four thermocouples are placed at top, bottom, or two sides of the pipe circumference with 180° or 90° apart. The outside surface temperature of the inner pipe T_w is then derived from the measured inside surface temperature by taking the radial heat conduction through the pipe wall into account.

The photographic apparatus established here to picture the qualitative characteristics of the evaporating flow in the annular duct consists of an IDT (X-Stream™ VISION XS-4) high-speed CMOS digital camera, a Mitutoyo micro-lens set, a 3-D positioning mechanism, a personal computer and a Nikon digital camera. The high-speed digital camera can take photographs up to 143,307 frames/s with an image resolution of 512×16. Here, a recording rate of 10,000 frames/s with the highest image resolution of 512×256 is adopted to obtain the images of the evaporating flow. The digital camera shutter speed can be as short as 1/4000 s in taking the overview of the flow. In particular, the flow pattern of the refrigerant in a small region around the middle axial location ($z = 80$ mm) is visualized. Note that the symbol z denotes the axial coordinate measuring from the inlet of the heated test section. After the experimental system reaches a statistically steady state, we start recording the evaporation activity. The high-speed digital camera can store the images which are later downloaded to a personal computer.

Before a test is started, the temperature of refrigerant R-134a in the test section is compared with its saturation temperature corresponding to the measured saturation pressure and the allowable difference is kept in the range of 0.2–0.3 K. Otherwise, the experimental system is re-evacuated and then re-charged to remove noncondensible gases existing in the refrigerant loop. In the test the liquid refrigerant at the inlet of the test section is first maintained at a specified temperature by adjusting the water-glycol temperature and flow rate. In addition, we adjust the thermostat temperature in the hot-water loop to stabilize the refrigerant temperature at the test section inlet. Next, the temperature and flow rate of the hot-water loop for the preheater are adjusted to keep the vapor quality of R-134a at the test section inlet at the desired value. Then, we regulate the refrigerant pressure at the test section

inlet by adjusting the opening of the gate valve locating right after the exit of the test section. Meanwhile, by changing the current of the DC motor connecting to the refrigerant pump, the refrigerant flow rate can be varied. The imposed heat flux from the heater to the refrigerant is adjusted by varying the electric current delivered from the programmable DC power supply to the electric heater. All tests are run at statistically steady-state conditions at which the time variations of the system pressure and imposed heat flux are, respectively, within ±1% and ±4% of their mean levels, and the time variations of the heated wall temperature are less than ±0.2 °C for a period of 100 min. Then all the data channels are scanned every 0.05 s for a period of 20 s.

3. Data reduction

The imposed heat flux to the refrigerant flow in the annular duct is calculated on the basis of the total power input Q_t and the total outside heat transfer area of the inner pipe of the annular duct A_s. The total power input is computed from the product of the measured voltage drop across the cartridge heater and the electric current passing through it. Hence the net power input to the test section Q_n is equal to $(Q_t - Q_{loss})$. The imposed heat flux at the outside surface of the inner pipe is then evaluated from the relation

$$q = Q_n/A_s \quad (1)$$

The total heat loss from the test section Q_{loss} is evaluated from the correlation for natural convection around a circular cylinder proposed by Churchill and Chu [14]. To reduce the heat loss from the test section, we cover the test section with a 2.5-cm thick polyethylene insulation layer. The results from the heat loss test indicate that the heat loss from the test section is generally less than 1% of the total power input no matter when a single-phase flow or a two-phase evaporating flow is in the duct. The average single-phase convection heat transfer coefficient for the refrigerant flow over the entire heated surface in the annular duct is defined as

$$h_l \equiv \frac{Q_n}{A_s \cdot (\overline{T}_w - T_{r,ave})} \quad (2)$$

where $T_{r,ave}$ is the average of the measured inlet and outlet temperatures of the refrigerant flow through the test section.

The vapor quality of R-134a entering the test section inlet is evaluated from the energy balance for the preheater. The total change of the refrigerant vapor quality in the test section is then deduced from the net heat transfer rate from the electric heater to the refrigerant in the test section. Finally, the circumferentially averaged heat transfer coefficient for the evaporation of R-134a at the middle axial location in the test section is determined from the definition

$$h_r \equiv \frac{Q_n}{A_s(\overline{T}_{wall} - T_{r,sat})} \quad (3)$$

More detailed description of the data reduction can be found from our earlier study [7]. Uncertainties of the heat transfer coefficients are estimated according to the procedures proposed by Kline and McClintock for the propagation of errors in physical measurement [15]. The results from this uncertainty analysis are summarized in Table 1.

4. Results and discussion

Results from the measured heat transfer data for the evaporation of R-134a in the narrow annular duct affected by the five experimental parameters, namely, the refrigerant mass flux, vapor quality, imposed heat flux, system pressure and duct size are presented here. The experiments are performed for the refrigerant mass flux varying from 300 to 700 kg/m^2 s with the imposed heat flux fixed at 5, 10, 15 kW/m^2 and system pressure set at 349.8 kPa, 414.6 kPa and 488.6 kPa (corresponding, respectively, to T_{sat} = 5, 10 and 15 °C). And the vapor quality at the middle axial location of the duct ranges from 0.05 to 0.95 for the annular gap of the duct δ = 1.0 and 2.0 mm. In what follows the effects of the experimental parameters on h_r for R-134a at the middle axial location are examined in detail. Besides, the results from visualizing the flow of R-134a evaporation in the duct will be inspected.

Table 1
Summary of results from the uncertainty analysis.

Parameter	Uncertainty
Annular duct geometry	
Length, width and thickness (%)	±1.0%
Gap size (%)	±5.0%
Area (%)	±2.0%
Parameter measurement	
Temperature, T (°C)	±0.2
Temperature difference, $\triangle T$ (°C)	±0.28
System pressure, P (MPa)	±0.002
Mass flux of refrigerant, G (%)	±2
Single-phase heat transfer	
Imposed heat flux, q (%)	±4.5
Heat transfer coefficient, h_l (%)	±12.5
Evaporation heat transfer	
Imposed heat flux, q (%)	±4.5
Mean vapor quality, x_m (%)	±9.5
Heat transfer coefficient, h_r (%)	±14

4.1. Single-phase heat transfer

Before beginning the evaporation experiments, the single-phase convective heat transfer tests are conducted for liquid R-134a flow in the annular duct. The measured h_l data are compared with the correlations proposed by Gnielinski [16] and Dittus–Boelter [17]. In the tests the refrigerant mass flux is varied from 220 to 1200 kg/m^2 s for the duct gap δ = 1.0 and 2.0 mm(corresponding to the Reynolds number of the refrigerant flow varying from 2668 to 15,412) at T_{sat} = 15 °C and inlet liquid subcooling ΔT_{sub} = 4 °C. Selected results from these tests are plotted in Fig. 2. The Gnielinski correlation is

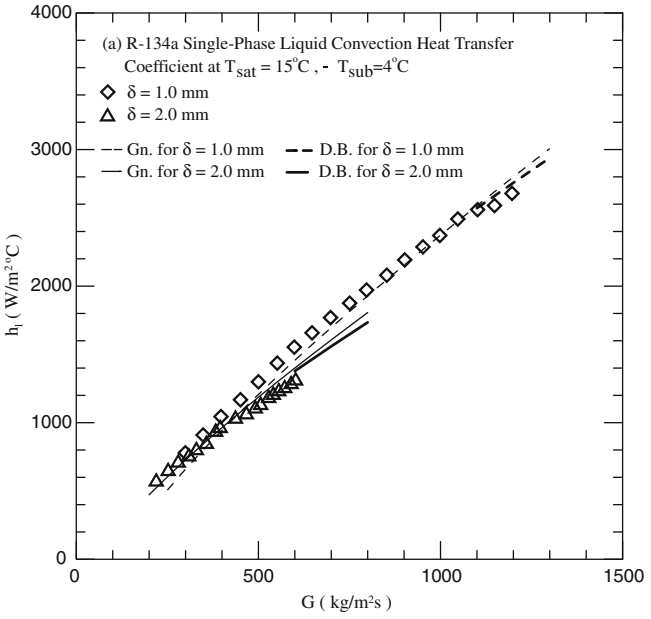

Fig. 2. Comparison of the present single-phase liquid convection heat transfer data h_l with the correlations of Gnielinski and Dittus–Boelter.

$$\mathrm{Nu}_l = \frac{(f_f/8)(\mathrm{Re}-1000)\mathrm{Pr}}{1+12.7\sqrt{f_f/8}(\mathrm{Pr}^{2/3}-1)} \tag{4}$$

applicable for $2300 < \mathrm{Re} < 10^6$ and $0.6 < \mathrm{Pr}_l < 10^5$, where

$$f_f = (1.82 \times \log_{10}\mathrm{Re} - 1.64)^{-2} \tag{5}$$

The Dittus–Boelter correlation is

$$\mathrm{Nu}_l = 0.023 \cdot \mathrm{Re}^{0.8} \cdot \mathrm{Pr}^{0.4} \tag{6}$$

applicable for $\mathrm{Re} > 10^5$ and $0.7 < \mathrm{Pr}_l < 16{,}700$

The above results manifest that the present data for the liquid R-134a forced convection in the narrow annular duct can be well correlated by their correlations. Thus the established system is considered to be suitable for the present R-134a evaporation experiment.

4.2. Evaporation heat transfer in narrow annular duct

At first, the heat transfer data for the R-134a evaporation for the duct gap of 2.0 mm are presented in Fig. 3 to illustrate the variations of the evaporation heat transfer coefficient at the middle axial location in the duct with the local vapor quality for various refrigerant mass fluxes, imposed heat fluxes and refrigerant saturated temperatures. These results indicate that for given q, T_{sat} and G the evaporation heat transfer coefficients increase almost linearly with the vapor quality, which is more prominent at a higher mass flux. The increase of h_r with $\boldsymbol{x}_m$ is considered to result from the fact that at a higher vapor quality the liquid film of the refrigerant on the heating surface becomes thinner. Hence the thermal resistance of the liquid film is reduced and heat transfer across the film is improved. Besides, at a higher vapor quality the mass flux of the vapor is larger and the vapor flow moves faster. This also improves the liquid–vapor interfacial heat transfer. To be more quantitative, the data in Fig. 3(a) show that at $q = 5\ \mathrm{kW/m^2}$, $G = 500\ \mathrm{kg/m^2\,s}$ and $T_{sat} = 15\ ^\circ\mathrm{C}$, the R-134a evaporation heat transfer coefficients at $\boldsymbol{x}_m = 0.07$ and 0.92 are, respectively, 1822 and 2837 $\mathrm{W/m^2{\circ}C}$. Hence an increase of 55.7% in h_r occurs for $\boldsymbol{x}_m$ raised from 0.07 to 0.92 for this case.

Then, the data shown in Fig. 3(a) manifest that the increase of h_r with the R-134a mass flux is rather significant except at low vapor quality. The increase in the evaporation heat transfer coefficient with the refrigerant mass flux is due to higher liquid and vapor velocities for a higher mass flux. Besides, the higher liquid and vapor speeds, respectively, in the liquid film and vapor core can promote the turbulence level in the refrigerant flow and we have stronger interfacial evaporation and better convection of the vapor flow over the liquid film. Thus a higher evaporation heat transfer coefficient results for a higher mass flux. Quantitatively, according to the data in Fig. 3(a) for $T_{sat} = 15\ ^\circ\mathrm{C}$ and $q = 5\ \mathrm{kW/m^2}$ the quality-averaged evaporation heat transfer coefficients for $G = 400$ and $500\ \mathrm{kg/m^2\,s}$ are $2016\ \mathrm{W/m^2{\circ}C}$ and $2345\ \mathrm{W/m^2{\circ}C}$, respectively. Thus, $\bar{h}_r$ is increased by 16.3% for the mass flux raised from 400 to $500\ \mathrm{kg/m^2\,s}$.

Next, the results presented in Fig. 3(b) indicate that the R-134a evaporation heat transfer coefficient rises with the saturated temperature of the refrigerant. This trend in the variation of h_r with T_{sat} is ascribed to the fact that at a higher T_{sat} the latent heat of vaporization i_{fg} is lower, which in turn results in a higher evaporation rate of the liquid R-134a. Hence, the R-134a vapor in the duct flows at a higher speed, producing a higher convection effect and therefore a higher h_r. To quantitatively illustrate the effects of T_{sat} on h_r, the quality-averaged evaporation heat transfer coefficients at $G = 500\ \mathrm{kg/m^2\,s}$ and $q = 15\ \mathrm{kW/m^2}$ are calculated from the data in Fig. 3(b). The results show that at $T_{sat} = 5$ and $15\ ^\circ\mathrm{C}$, the heat transfer coefficients are about $3079\ \mathrm{W/m^2{\circ}C}$ and $3797\ \mathrm{W/m^2\,{\circ}C}$, respectively. Thus for T_{sat} raised from 5 to 15 °C, $\bar{h}_r$ is increased by 23.3%.

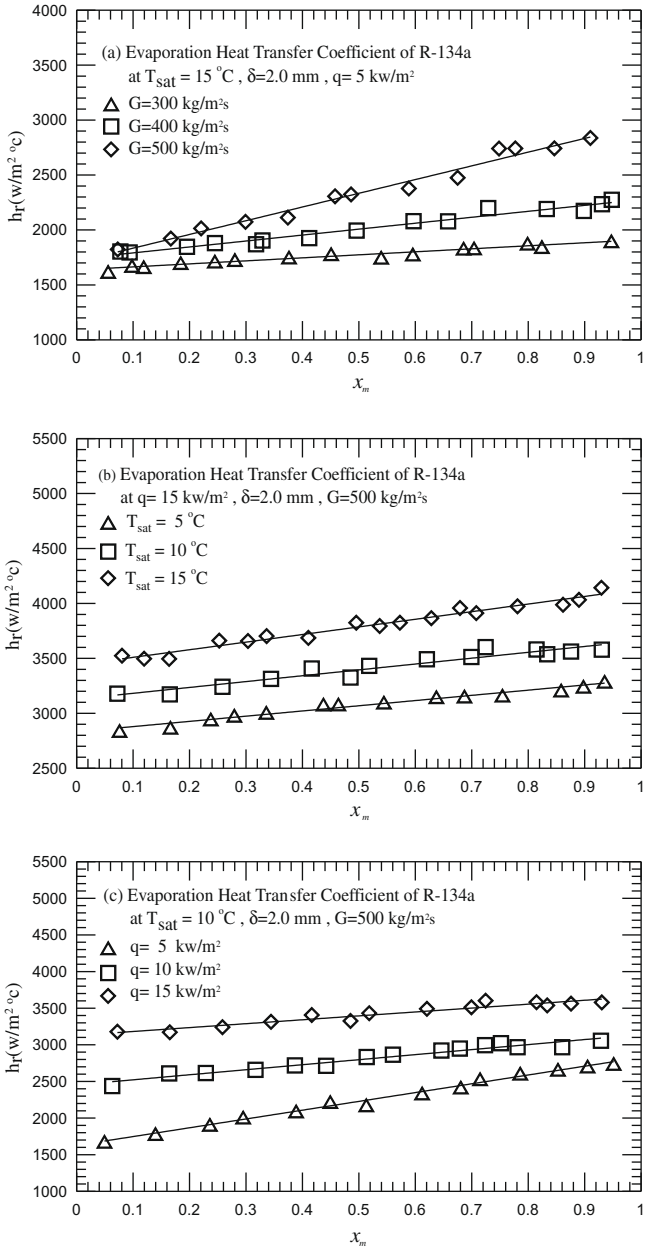

Fig. 3. Variations of R-134a evaporation heat transfer coefficient with vapor quality at $\delta = 2.0$ mm : (a) for various G at $T_{sat} = 15\ ^\circ\mathrm{C}$ and $q = 5\ \mathrm{kW/m^2}$, (b) for various T_{sat} at $q = 15\ \mathrm{kW/m^2}$ and $G = 500\ \mathrm{kg/m^2\,s}$ and (c) for various q at $T_{sat} = 10\ ^\circ\mathrm{C}$ and $G = 500\ \mathrm{kg/m^2\,s}$.

Finally, based on the data shown in Fig. 3(c) for $\delta = 2.0$ mm the R-134a evaporation heat transfer coefficient increases rather significantly with the imposed heat flux for various T_{sat} and G especially at low vapor quality. This significant increase of h_r with q reflects that the R-134a evaporation at the liquid–vapor interface in the refrigerant flow is substantially augmented by the increase in the imposed heat flux. Besides, at low vapor quality bubble nucleation on the heated surface is more important in the refrigerant flow which will be discussed later. Thus raising the imposed heat flux can enhance the active bubble nucleation density, bubble generation frequency and bubble growth, causing h_r to increase more significantly with q at low vapor quality. According to the data in Fig. 3(c) for $T_{sat} = 10\ ^\circ\mathrm{C}$ and $G = 500\ \mathrm{kg/m^2\,s}$, the quality-averaged evaporation heat transfer coefficients for $q = 5$ and $15\ \mathrm{kW/m^2}$ are 2277 and $3424\ \mathrm{W/m^2\,{\circ}C}$, individually. Thus for q raised from 5 to $15\ \mathrm{kW/m^2}$ $\bar{h}_r$ is increased by 50.4%.

Attention is then turned to examining the heat transfer data for the R-134a evaporation for the smaller duct gap of 1.0 mm. The data for δ = 1.0 mm measured here are presented in Fig. 4. Comparing these results with that in Fig. 3 for δ = 2.0 mm indicates that the effects of the refrigerant vapor quality, mass flux and saturated temperature, and the imposed heat flux on the R-134a evaporation heat transfer coefficient are similar for both δ = 1.0 and 2.0 mm. A close inspection of these data, however, reveals that some differences do exist. To be more clear, we show the data for δ = 1.0 and 2.0 mm together in Figs. 5 and 6. The results in Figs. 5 and 6 manifest that h_r is significantly better for δ = 1.0 mm for the same G, q and T_{sat}. Quantitatively, Fig. 5(c) shows that the quality-averaged evaporation heat transfer coefficients for δ = 1.0 and 2.0 mm at G = 500 kg/m^2 s, T_{sat} = 15 °C and q = 5 kW/m^2 are 2875 and 2345 W/m^2 °C, respectively. An increase of 22.6% in $\bar{h}_r$ occurs for

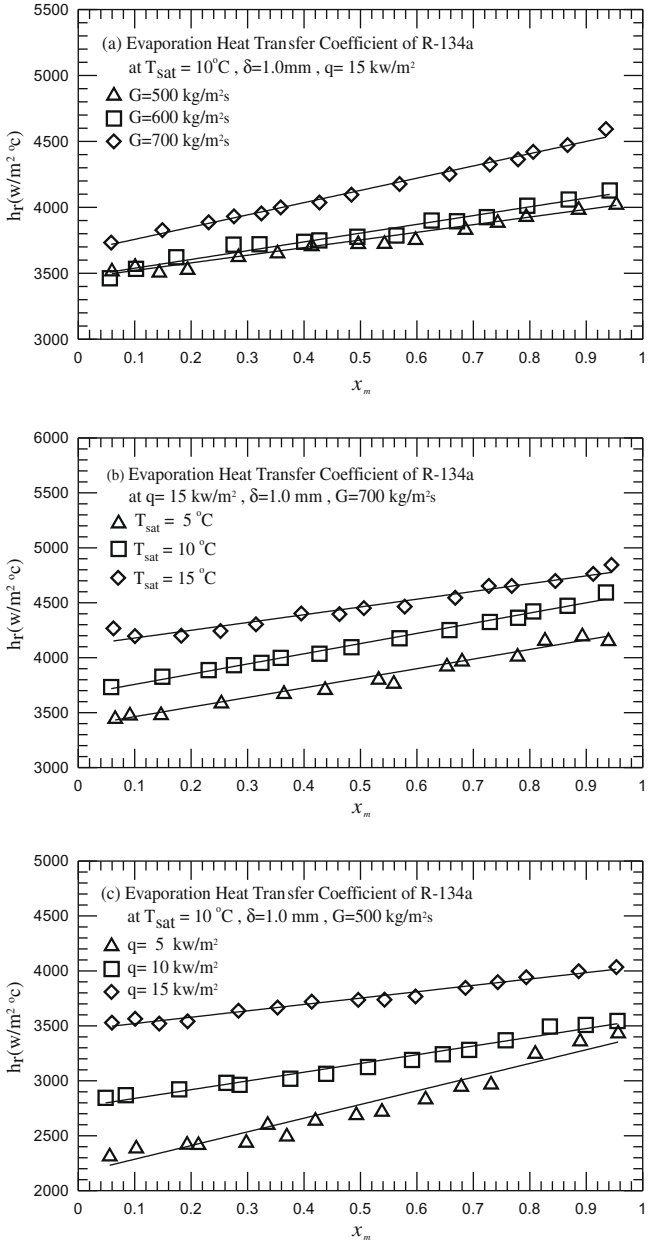

Fig. 4. Variations of R-134a evaporation heat transfer coefficient with vapor quality at δ = 1.0 mm : (a) for various G at T_{sat} = 10 °C and q = 15 kW/m^2, (b) for various T_{sat} at q = 15 kW/m^2 and G = 700 kg/m^2 s and (c) for various q at T_{sat} = 10 °C and G = 500 kg/m^2 s.

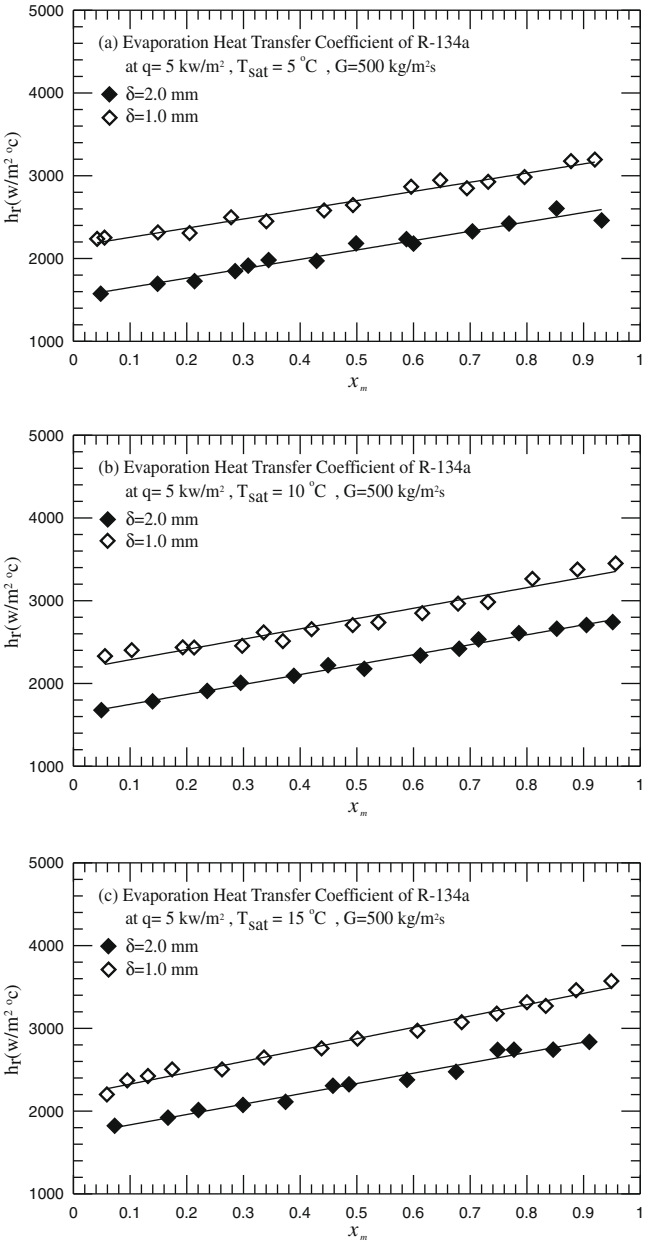

Fig. 5. Variations of R-134a evaporation heat transfer coefficient with vapor quality at q = 5 kW/m^2 and G = 500 kg/m^2 s for various δ for (a) T_{sat} = 5 °C, (b) T_{sat} = 10 °C and (c) T_{sat} = 15 °C.

δ reduced from 2.0 mm to 1.0 mm. This increase in h_r at reducing δ can be attributed to the fact that at a smaller gap the average liquid film thickness is thinner. Hence the thermal resistance of the liquid film is reduced and heat transfer across the film is improved.

Besides, contrasting the results in Fig. 4 for δ = 1.0 mm with that in Fig. 3 for δ = 2.0 mm suggests that the refrigerant mass flux shows milder effects on h_r in the narrower duct for q = 5 and 10 kW/m^2, as evident from the data shown in Fig. 6(a). According to the data in Fig. 4(a) for T_{sat}=10 °C and q = 15 kW/m^2 the quality-averaged evaporation heat transfer coefficients for G = 600 and 700 kg/m^2 s are 3801 W/m^2 °C and 4139 W/m^2 °C, respectively. Thus, $\bar{h}_r$ is only increased by 8.8% in the narrower duct with δ = 1.0 mm for the R-134a mass flux raised from 600 to 700 kg/m^2 s.

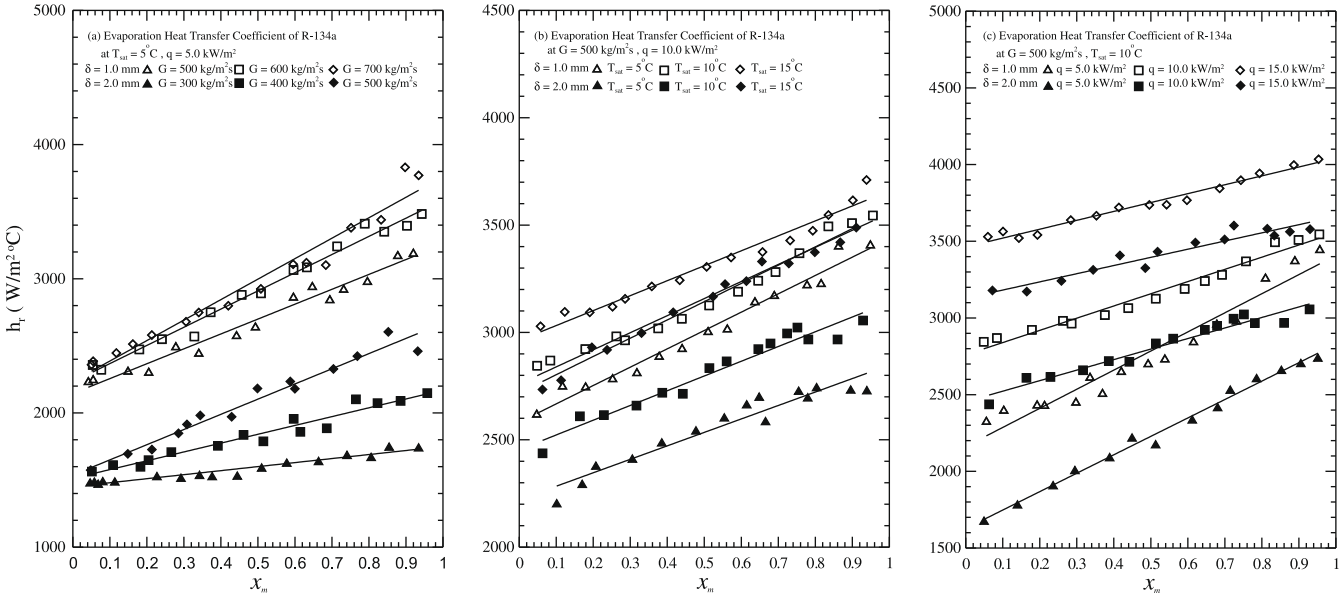

Fig. 6. Variations of R-134a evaporation heat transfer coefficient with vapor quality for various δ: for (a) various G at T_{sat} = 5 °C and q = 5 kW/m^2, (b) various T_{sat} at G = 500 kg/m^2 s and q = 10 kW/m^2 and (c) various q at T_{sat} = 10 °C and G = 500 kg/m^2 s.

Moreover, a comparison of the data for δ = 1.0 and 2.0 mm manifests that at low and intermediate imposed heat fluxes for q = 5 and 10 kW/m^2 the effects of the refrigerant saturated temperature on the R-134a evaporation heat transfer coefficient are slightly less pronounced in the narrower duct. This can be more clearly seen in Fig. 6(b). Quantitatively, the quality-averaged evaporation heat transfer coefficients at G = 700 kg/m^2 s and q = 15 kW/m^2 are calculated from the data in Fig. 4 (b) for δ = 1.0 mm. The results show that at T_{sat} = 5, 10 and 15 °C, the heat transfer coefficients are about 3826, 4138 and 4472 W/m^2 °C, respectively. Thus for T_{sat} raised from 5 to 15 °C, $\bar{h}_r$ is increased by 16.9%.

Furthermore, the data shown in Fig. 4 for δ = 1.0 mm, when contrasted with that in Fig. 3 for δ = 2.0 mm, indicate that in the narrower duct the effects of the imposed heat flux on the R-134a evaporation heat transfer coefficient are slightly weaker, as clearly seen from the data given in Fig. 6(c). According to the data in Fig. 4(c) for T_{sat} = 10 °C and G = 500 kg/m^2 s, the quality-averaged evaporation heat transfer coefficients for q = 5, 10 and 15 kW/m^2 are 2761, 3161 and 3743 W/m^2 °C, individually. Thus for q raised from 5 to 15 kW/m^2 $\bar{h}_r$ is increased by 35.6% for δ = 1.0 mm.

4.3. Characteristics of R-134a evaporating flow in narrow annular duct

In addition to the heat transfer data presented above, the photos of the R-134a evaporating flow taken from the duct side over the entire duct and over a small region around the middle axial location are shown in Figs. 7–11 for selected cases. The mean void fraction α_m and liquid film thickness t_{lf} at the middle axial location given in the figures are estimated from the separated two-phase flow model proposed by Lockhart and Martinelli [18]. The flow photos shown in Figs. 7–9 for δ = 2.0 mm indicate that at the low vapor quality of 0.05 bubble nucleation on the heating surface can be seen only at some locations at the low imposed heat flux of 5 kW/m^2. But at the much higher q of 15 kW/m^2 the bubble nucleation density is rather high at this low $\boldsymbol{x}_m$. This apparently results from the fact that the heating surface is entirely covered by the liquid R-134a at $\boldsymbol{x}_m$ = 0.05. Merging of small bubbles into large bubbles takes place frequently. Some bubbles are relatively large. Actually, they can be regarded as bubble slugs. Besides, bubbles dispersed in a large liquid slug appear in the duct. Moreover, due to the gravity effects the top and bottom parts of the duct are, respectively, dominated by the vapor and liquid flows. At the intermediate vapor quality of 0.54 some bubble nucleation on the heating surface can also be seen at a high q. Beyond the inlet region the flow in the duct is dominated by the vapor flow over thin liquid film around the inner pipe and it is an annular two-phase flow. Irregular moving waves appear at the vapor–liquid interface. We also observe a small liquid slug. In the entrance region of the duct, bubbles interdisperse with liquid and both move irregularly. Coalescence of bubbles as they move downstream resulting in the annular flow. It is of interest to note that at the very high vapor quality of 0.94 bubble nucleation can still be seen at q = 15 kW/m^2 although the liquid film covering the heating surface is very thin. Again at this high quality the duct is dominated by the annular two-phase flow except in the entrance region. At the vapor–liquid interface irregular waves still prevail. But no liquid slug exists.

Next, the effects of the experimental parameters on the global evaporating flow pattern are examined. Comparing the results in Figs. 7 and 8 indicates that at the higher imposed heat flux a bigger liquid slug forms at $\boldsymbol{x}_m$ = 0.05 and at $\boldsymbol{x}_m \geqq$ 0.54 the annular flow prevails in a larger portion of the duct. For a lowering of the refrigerant saturated temperature from 15 °C to 5 °C, at $\boldsymbol{x}_m$ = 0.05 the liquid slug becomes larger due to less bubble nucleation at the lower T_{sat}, as evident from the photos in Figs. 8 and 9. Note that a number of bubbles disperse in the liquid slug. We also note that at $\boldsymbol{x}_m$ = 0.94 for T_{sat} = 5 °C the annular flow exists almost in the entire duct (Fig. 9(c)). As the refrigerant mass flux is raised from 300 to 400 kg/m^2 s, less bubbles nucleate on the heating surface. This results in the disappearance of the liquid slug at low $\boldsymbol{x}_m$ and a smaller region of annular flow in the duct for G = 400 kg/m^2 s at T_{sat} = 15 °C.

Finally, the photos of the evaporating flow in the narrower duct (δ = 1.0 mm) are presented in Fig. 10. The effects of the vapor quality, imposed heat flux and refrigerant mass flux and saturated temperature on the evaporating flow for δ = 1.0 mm are qualitatively similar to that for δ = 2.0 mm. The duct gap, however, exhibits some important influences. Contrasting the flow photos for δ = 1.0 mm in Fig. 10 with that in Fig. 11 for δ = 2.0 mm at the same G(=500 kg/m^2 s), T_{sat} (=15 °C) and q(=5 kW/m^2) reveals that in the narrower duct the bubble coalescence is more frequent and we

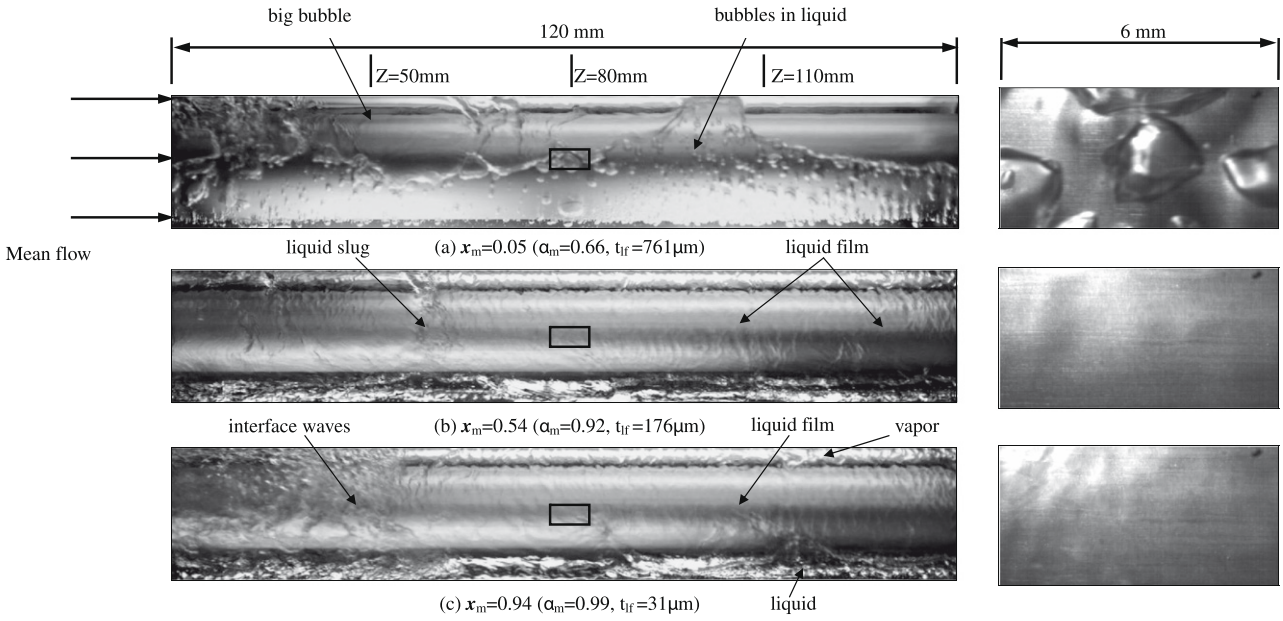

Fig. 7. Photos of flow in the evaporation of R-134a in the entire duct and a small region around middle axial location at G = 300 kg/m^2 s, T_{sat} = 15 °C, δ = 2.0 mm, q = 5 kW/m^2 for (a) x_m = 0.05, (b) x_m = 0.54 and (c) x_m = 0.94.

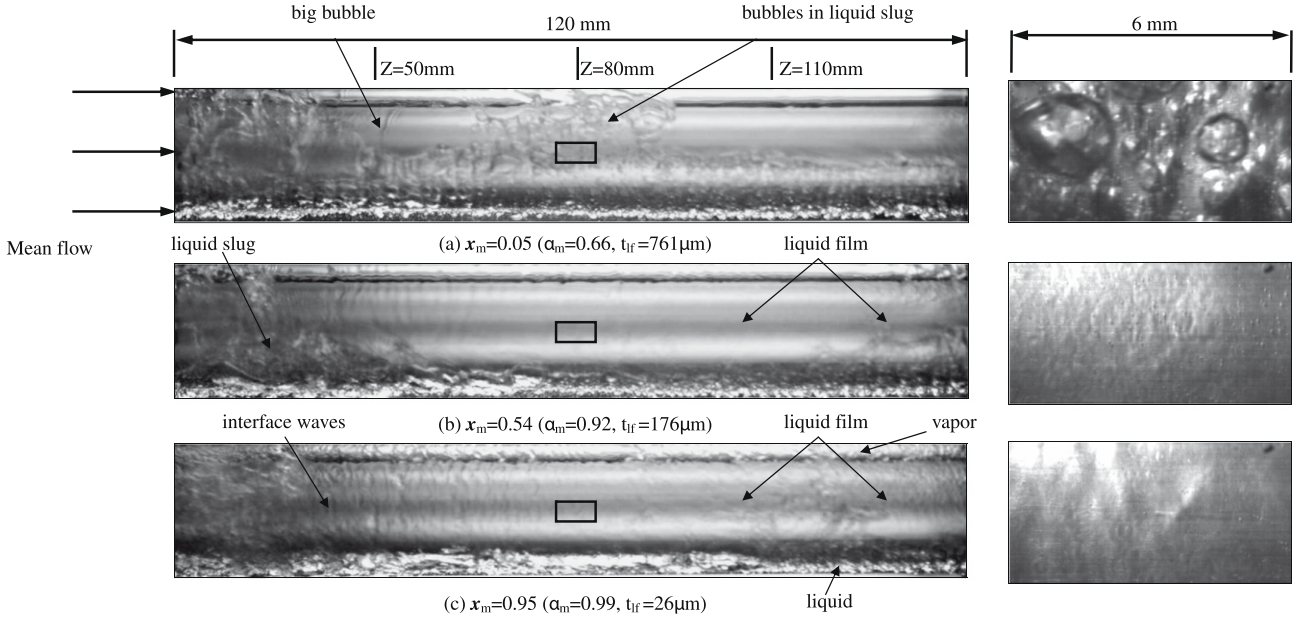

Fig. 8. Photos of flow in the evaporation of R-134a in the entire duct and a small region around middle axial location at G = 300 kg/m^2 s, T_{sat} = 15 °C, δ = 2.0 mm, q = 15 kW/m^2 for (a) x_m = 0.05, (b) x_m = 0.54 and (c) x_m = 0.95.

have more big bubbles in the duct at low $\boldsymbol{x}_m$. Besides, at high $\boldsymbol{x}_m$ annular two-phase flow regions interrupted by liquid slugs prevail for δ = 1.0 mm.

4.4. Correlation equation for evaporation heat transfer coefficient

To facilitate the design of air-conditioning systems, the present heat transfer data for the R-134a evaporation in the narrow annular duct are correlated empirically. The data presented above indicate that h_r varies linearly with the vapor quality at the middle axial location and the correlation is thus expressed as

$$\mathrm{Nu_r} = \frac{h_r \cdot D_h}{k_l} = m_1 \boldsymbol{x}_m + m_2 \tag{7}$$

where m_1 and m_2 are chosen as

$$m_1 = f(\mathrm{Bo}, \mathrm{Re}) = a_1 + b_1 \mathrm{Bo}^{c_1} \mathrm{Re}^{d_1} \tag{8}$$

$$m_2 = f(\mathrm{Bo}, \mathrm{Re}) = a_2 \mathrm{Bo}^{b_2} \mathrm{Re}^{c_2} \tag{9}$$

The values for the coefficients in the above equatiions are a_1 = 30, b_1 = 0.187, c_1 = 2.9, d_1 = 3.09, a_2 = 24.7, b_2 = 0.68 and c_2 = 0.855. The Boiling number and Reynolds number for the flow are defined, respectively, as

$$\mathrm{Bo} = \frac{q}{G \cdot i_{fg}} \tag{10}$$

$$\mathrm{Re} = \frac{G \cdot D_h}{\mu_l} \tag{11}$$

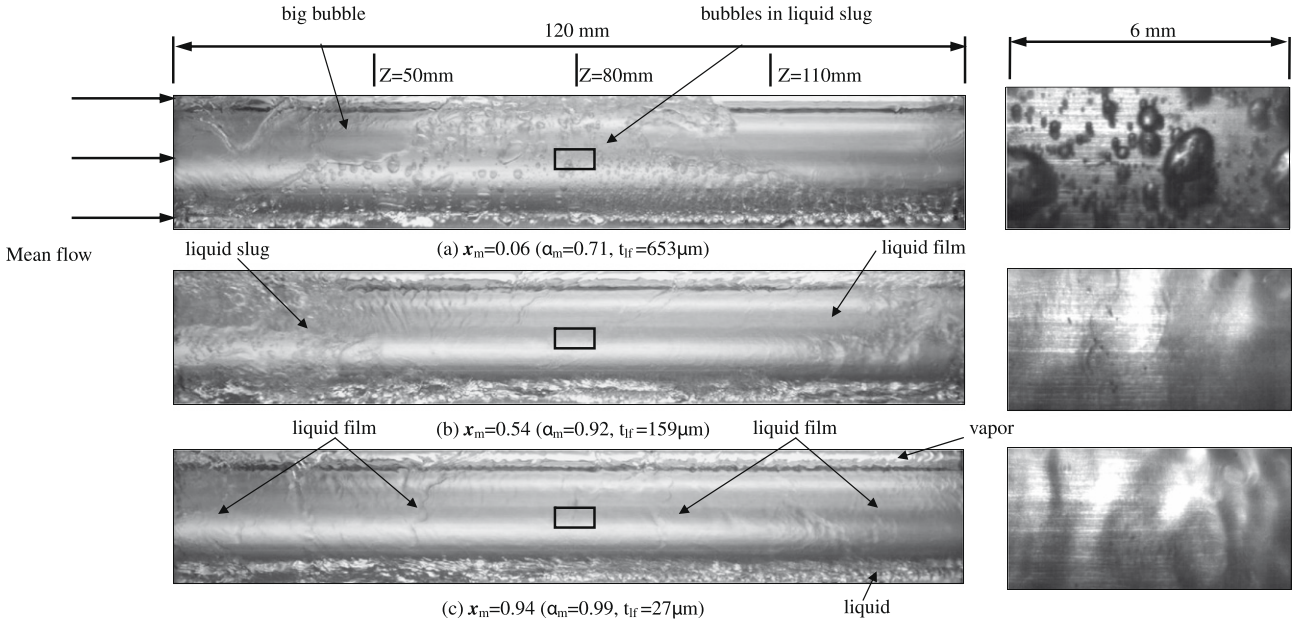

Fig. 9. Photos of flow in the evaporation of R-134a in the entire duct and a small region around middle axial location at G = 300 kg/m^2 s, T_{sat} = 5 °C, δ = 2.0 mm, q = 15 kW/m^2 for (a) x_m = 0.06, (b) x_m = 0.50 and (c) x_m = 0.94.

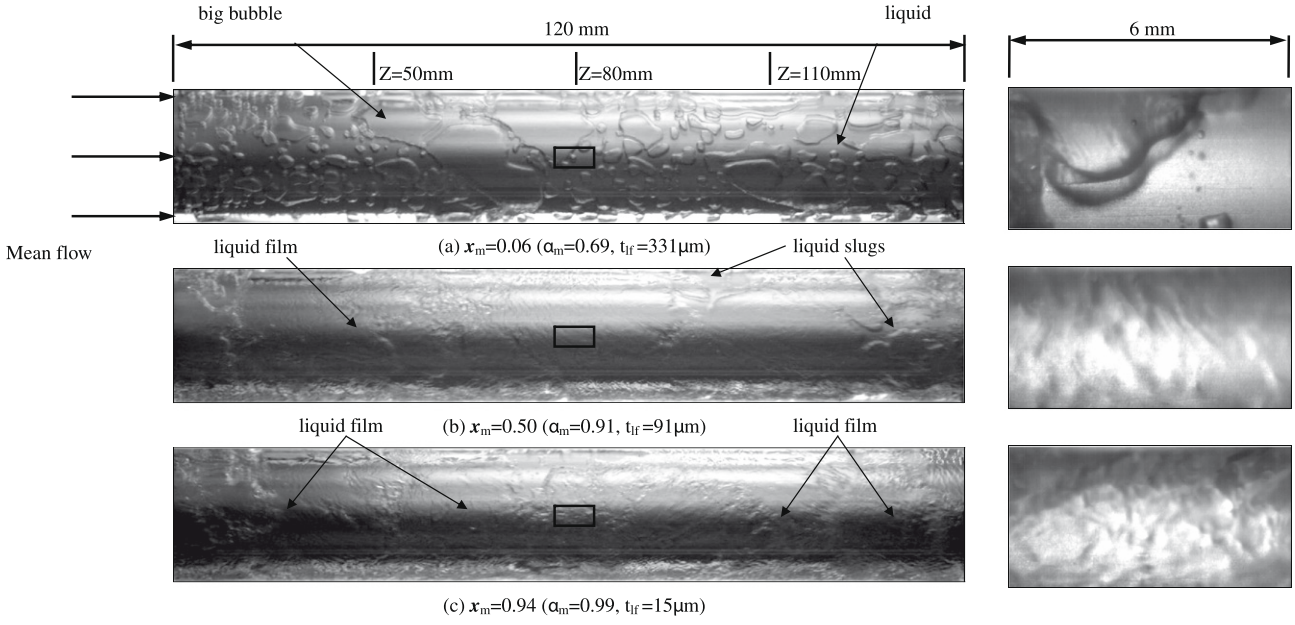

Fig. 10. Photos of flow in the evaporation of R-134a in the entire duct and a small region around middle axial location at G = 500 kg/m^2 s, T_{sat} = 15 °C, δ = 1.0 mm, q = 5 kW/m^2 for (a) x_m = 0.06, (b) x_m = 0.50 and (c) x_m = 0.94.

Comparison of the above correlation with the present experimental data shown in Fig. 12 indicates that more than 96% of the present data for h_r fall within ±25% of Eq. (7), and the mean absolute error (MAE) between the present data for h_r and the proposed correlation for the R-134a evaporation in the narrow ducts is 10.3%.

5. Concluding remarks

In this study, we have experimentally measured the heat transfer coefficient and visualized the two-phase flow pattern for the R-134a evaporation in the horizontal narrow annular ducts with δ = 1.0 and 2.0 mm. The effects of the refrigerant vapor quality, saturated temperature, mass flux, imposed heat flux and gap size on the evaporation heat transfer coefficient at the middle axial location of the duct have been examined in detail. A summary of the major findings is given in the following.

(1) The R-134a evaporation heat transfer coefficient in the narrow ducts increases almost linearly with the vapor quality and the increase is more significant at a higher refrigerant mass flux. Besides, increases in the refrigerant mass flux and saturated temperature and imposed heat flux can substantially improve the evaporation heat transfer. The effects of G and T_{sat} on h_r are less pronounced for δ = 1.0 mm.
(2) Reducing the gap size of the duct causes a significant increase in the R-134a evaporation heat transfer coefficient.

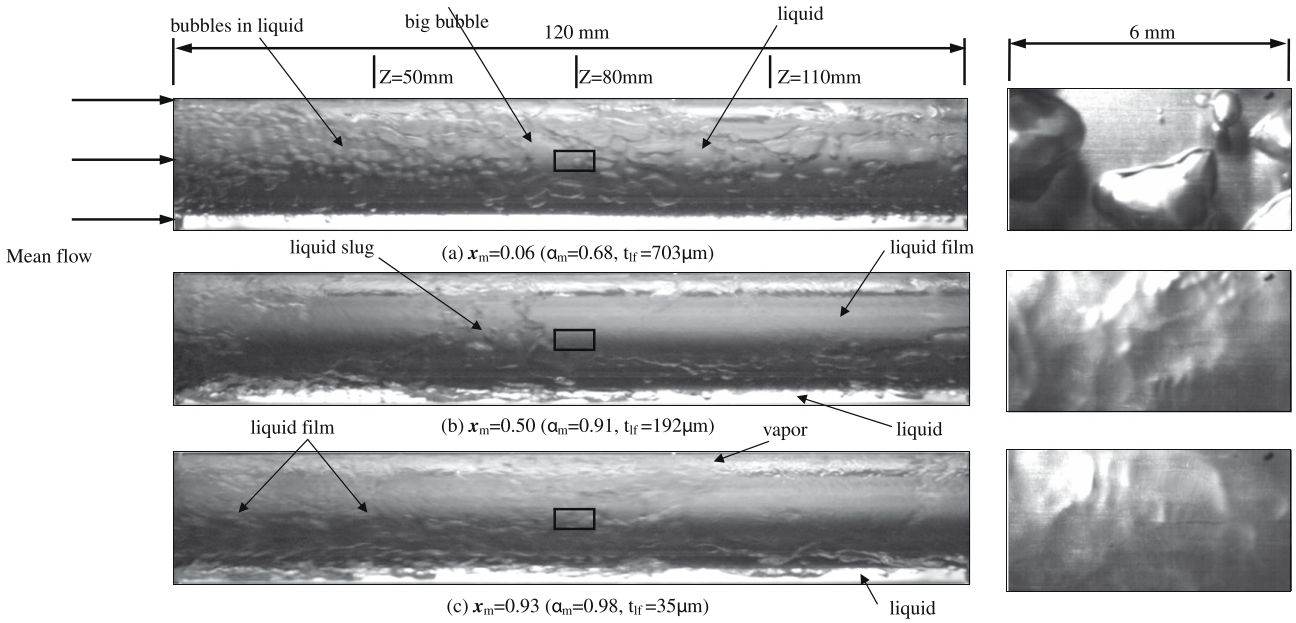

Fig. 11. Photos of flow in the evaporation of R-134a in the entire duct and a small region around middle axial location at G = 500 kg/m^2 s, T_{sat} = 15 °C, δ = 2.0 mm, q = 5 kW/m^2 for (a) x_m = 0.05, (b) x_m = 0.50 and (c) x_m = 0.93.

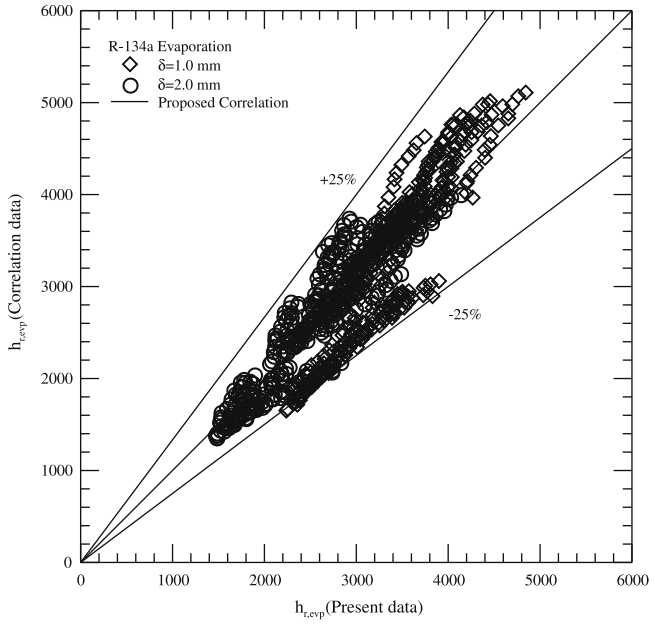

Fig. 12. Comparison of the measured data for heat transfer coefficient for the evaporation of R-134a in the narrow ducts with the proposed correlation.

(3) In the flow visualization the bubble nucleation on the heating surface is found to be important at low vapor quality. Besides, at low vapor quality merging of small bubbles to form big bubbles and merging of big bubbles into bubble slugs take place, which is more pronounced at the smaller duct gap. Moreover, bubbles dispersed in a large liquid slug appear in the duct. At the intermediate vapor quality some bubble nucleation on the heating surface also exists and the flow in the duct is dominated by the vapor flow over thin liquid film around the inner pipe, an annular two-phase flow. Irregular waves appear at the vapor–liquid interface. At the very high vapor quality bubble nucleation can still be seen at high imposed heat flux. At this high quality the duct is also dominated by the annular two-phase flow. The annular two-phase flow prevails in a larger portion of the duct at higher imposed flux, lower refrigerant mass flux and higher refrigerant saturated temperature.

(4) Empirical equation to correlate the present heat transfer data for the R-134a evaporation in the annular ducts is provided.

Acknowledgments

The financial support of this study by the engineering division of National Science Council of Taiwan, ROC through the contract NSC 96-2221-E-009-133-MY3 is greatly appreciated.

References

[1] S.G. Kandlikar, Fundamental issues related to flow boiling in minichannels and microchannels, Exp. Thermal Fluid Sci. 26 (2002) 389–407.
[2] S.G. Kandlikar, W.J. Grande, Evolution of microchannel flow passages – thermohydraulic performance and fabrication technology, Heat Transfer Eng. 24 (1) (2003) 3–17.
[3] P.A. Kew, K. Cornwell, Correlations for the prediction of boiling heat transfer in small-diameter channels, Appl. Therm. Eng. 17 (1997) 705–715.
[4] C.C. Wang, C.S. Chiang, Two-phase heat transfer characteristics for R-22/R-407C in a 6.5-mm smooth tube, Int. J. Heat Fluid Flow 18 (1997) 550–558.
[5] C.Y. Park, P.S. Hrnjak, CO_2 and R-410A flow boiling heat transfer, pressure drop, and flow pattern at low temperatures in a horizontal smooth tube, Int. J. Refrig. 30 (2007) 166–178.
[6] B. Watel, Review of saturated flow boiling in small passages of compact heat-exchangers, Int. J. Therm. Sci. 42 (2) (2003) 107–140.
[7] Y.Y. Yan, T.F. Lin, Evaporation heat transfer and pressure drop of refrigerant R-134a in a small pipe, Int. J. Heat Mass Transfer 41 (1998) 4183–4194.
[8] Y.Y. Yan, T.F. Lin, Reply to Prof. R.L. Webb's and Dr. J.W. Paek's comments, Int. J. Heat Transfer 46 (6) (2003) 1111–1113.
[9] R. Yun, Y. Kim, M.S. Kim, Convective boiling heat transfer characteristics of CO_2 in microchannels, Int. J. Heat Mass Transfer 48 (2005) 235–242.
[10] Y.M. Lie, F.Q. Su, R.L. Lai, T.F. Lin, Experimental study of evaporation heat transfer characteristics of refrigerants R-134a and R-407C in horizontal small tubes, Int. J. Heat Mass Transfer 49 (2006) 207–218.
[11] R. Yun, J.H. Heo, Y. Kim, Evaporative heat transfer and pressure drop of R410A in microchannels, Int. J. Refrig. 29 (2006) 92–100.
[12] K.I. Choi, A.S. Pamitran, C.Y. Oh, J.T. Oh, Boiling heat transfer of R-22, R-134a, and CO2 in horizontal smooth minichannels, Int. J. Refrig. (2007) 1–11.

[13] Y.M. Lie, T.F. Lin, Saturated flow boiling heat transfer and associated bubble characteristics of R-134a in a narrow annular duct, Int. J. Heat Mass Transfer 48 (25–26) (2005) 5602–5615.
[14] S.W. Churchill, H.H.S. Chu, Correlating equations for laminar and turbulent free convection from a horizontal cylinder, Int. J. Heat Mass Transfer 18 (1975) 049–1053.
[15] S.J. Kline, F.A. McClintock, Describing uncertainties in single-sample experiments, Mech. Eng. 75 (1) (1953) 3–12.
[16] V. Gnielinski, New equations for heat and mass transfer in turbulent pipe and channel flow, Int. Chem. Eng. 16 (2) (1976) 359–368.
[17] F.W. Dittus, L.M.K. Boelter, Heat Transfer in Automobile Radiator of the Tube Type Publication in Engineering, vol. 2, University of California, Berkley, 1930. pp. 250.
[18] R.W. Lockhart, R.C. Martinelli, Proposed correlation of data for isothermal two-phase two-component flow in pipes, Chem. Eng. Prog. 45 (1949) 39–48.